Available online at www.sciencedirect.com
ScienceDirect
Scripta Materialia 60 (2009) 68–71
Scripta MATERIALIA
www.elsevier.com/locate/scriptamat

Unusual wavy weld pool boundary from dimensional analysis

A. Arora,[a] G.G. Roy[b] and T. DebRoy[a,*]

[a] *Department of Materials Science and Engineering, The Pennsylvania State University, University Park, Penn State University, 115 Steidle Building, PA 16802, USA*
[b] *Indian Institute of Technology, Kharagpur, India*

Received 6 August 2008; revised 30 August 2008; accepted 30 August 2008
Available online 9 September 2008

The geometry of a weld pool affects its solidification behavior. Here we show that the welding parameters and material properties responsible for the formation of unusual, wavy fusion boundaries can be identified from heat and fluid flow calculations and confirmed by independent experiments. These parameters and properties can be expressed by dimensionless numbers using the Buckingham π-theorem. The wavy boundary originates from the interaction of counter-rotating liquid metal loops at high Marangoni numbers. The Prandtl number affects the type of inflection.

Keywords: Welding; Modeling; Fusion boundary

Two important factors affecting the solidification of weld metal are the temperature gradient (G) and the solidification growth rate (R). The scale of the solidification structure is affected by the cooling rate (GR) and the morphology of the structure depends on G/R. [1] Since the values of both G and R are affected by the geometry of the fusion boundary, both the solidification structure and the morphology are affected by the nature of the fusion boundary. In most cases, the fusion boundary shape is similar to a hemisphere. However, in some cases, the shape is much more complex than a simple hemisphere. Depending on welding variables and material properties, the fusion boundary can be wavy with multiple inflections of its slope. Figure 1 shows examples of the three different shapes of the weld pool fusion boundary. Figure 1a shows the common hemispherical fusion boundary [2], and Figure 1b and c show two much less common fusion boundaries, both wavy in nature and containing multiple inflections of the slope of the boundary [3–5].

The influence of the geometry of the fusion boundary on both the solidification structure, [6] and, for certain alloys, solidification crack formation probability [7], has been studied. Liu and DuPont [6] examined the effect of weld pool geometry on the dendrite growth direction and velocity during laser melting of single-crystal nickel-base CMSX-4 superalloy. They reported a critical slope of the fusion boundary below which unidirectional dendrite growth along [0 0 1] can be achieved. When the slope is higher than the critical value, dendrite growth may occur along the [1 0 0], [0 1 0] and [0 $\bar{1}$ 0] directions. Wolf et al. [7] showed experimentally that high curvatures of the solidification front result in a high rate of shrinkage and a high probability of solidification cracking for certain alloys. Mendez and Eager [8] used a non-dimensional system of equations for arc welding to explain the finger-like penetration and hump bead formation. Fuerschbach [9] developed a dimensionless parameter model for linear laser and arc welds to predict the cross-sectional area of the weld. Drezet et al. [10,11] suggested that a wavy fusion zone boundary appeared when the weld pool width was larger than the laser beam radius. Its appearance was thought to result from the effect of Marangoni eddies. Limmaneevichitr and Kou [3] showed that the weld pool shape could be explained by using the Peclet number which represents the ratio of heat transfer rates by convection and conduction. They showed that welds with low Peclet number exhibit a concave bottom, and the bottom becomes flat and even convex with increase in Peclet number. However, the Peclet number does not explicitly include any welding parameters. A critical review of the literature shows that the importance of the fusion boundary shape is well recognized but a mechanistic understanding of the formation of the wavy fusion boundary, and consequently the conditions for its formation, are not known.

Here we show that the welding conditions and material properties responsible for the formation of the wavy boundary can be identified using a heat and fluid flow

* Corresponding author. Tel.: + 1 814 865 1974; e-mail: debroy@psu.edu

1359-6462/$ - see front matter © 2008 Acta Materialia Inc. Published by Elsevier Ltd. All rights reserved.
doi:10.1016/j.scriptamat.2008.08.035

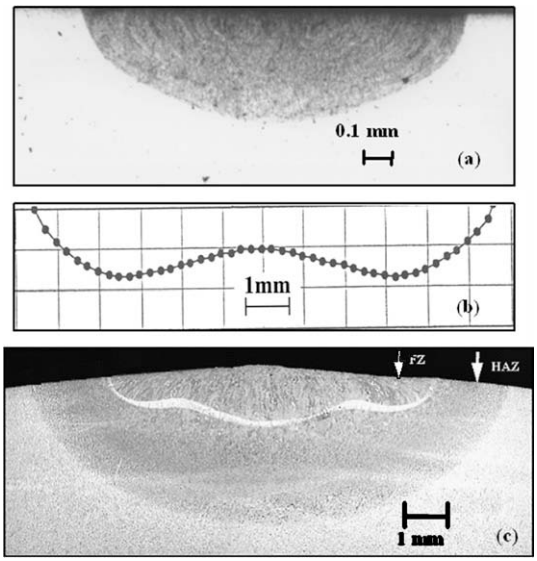

Figure 1. Examples of different shapes of fusion boundary: (a) arc welding of Al alloy 5182 [2]; (b) laser melting of $NaNO_3$ [3,4]; (c) arc spot welding of steel [5].

model and expressed by dimensionless numbers based on the Buckingham π-theorem.

A well-tested three-dimensional heat transfer and fluid flow model [12–17] was used to calculate temperature and velocity fields in the weld pool for a wide range of material properties and welding parameters. The calculated temperature fields were used to determine the weld pool geometry from the solidus temperature contour in any selected section of the weld pool. The Buckingham π-theorem was used to determine the appropriate dimensionless parameters containing the welding variables and material properties that affect the welding process.

If a system can be defined with n variables which can be expressed in terms of m fundamental units, namely mass (M), length (L), time (T), temperature (θ), the system can be defined with the help of n-m dimensionless numbers [18]. Of the nine variables that affect the weld pool geometry, the power distribution factor is dimensionless and is excluded from the dimensionless analysis. Since the remaining eight variables were expressed by four independent fundamental units as shown in Table 1, the system can be defined by four dimensionless numbers. Based on four primary variables, R, ρ, T_m and μ, the four dimensionless numbers are derived as shown in Table 2. The first three dimensionless numbers, π_1, π_2 and π_3, may be combined to yield two meaningful dimensionless numbers, namely the Prandtl (Pr) and Marangoni (Ma) numbers. The Prandtl number Pr $\left[=\frac{\mu C_P}{k}\right]$, represents the relative rates of viscous momentum transfer to heat conduction. The Marangoni number Ma $\left[=\frac{\rho C_P R\frac{d\gamma}{dT}(T_P-T_m)}{k\mu}\right]$ represents the relative importance of surface tension force to viscous force and indicates the strength of the Marangoni flow. Since the surface tension force depends on the temperature gradient on the surface, $(T_P–T_m)$ is more meaningful than T_m, where T_p represents the peak temperature. The ratio of two dimensionless numbers, π_2 and π_4, gives a meaningful dimensionless number Q^* $\left[=\frac{Q}{RkT_m}\right]$ representing dimensionless heat input which is the ratio of heat supply rate and the conduction heat transfer rate. Therefore, we have three meaningful dimensionless numbers, Pr, Ma and Q^* which are used to study the wavy pool shape.

Table 1. Dimensions of variables in the MLT θ system

Power absorbed	Q	$M L^2 T^{-3}$
Radius of the heat source	R	L
Melting temperature	T_m	θ
Effective viscosity of liquid metal	μ	$M L^{-1} T^{-1}$
Temperature coefficient of surface tension	$d\gamma/dT$	$M T^{-2} \theta^{-1}$
Effective thermal conductivity of liquid	k	$M L T^{-3} \theta^{-1}$
Density of liquid metal	ρ	$M L^{-3}$
Specific heat of liquid	C_P	$L^2 T^{-2} \theta^{-1}$

Figure 1a shows a commonly observed hemispherical weld pool shape [2] for an arc spot weld of aluminum alloy 5182 (4.2% Mg, 0.2% Si, 0.35% Mn, 0.1% Cr, 0.15% Sn, 0.07% Zn, 0.1% Ti and rest Al), while Figure 1b and c show very unusual fusion zone shapes with multiple inflections in the slope of the boundaries for sodium nitrate ($NaNO_3$) [3] and steel (0.23% C, 0.5% Mn, 1.7% Al, 0.28% Si, 0.02% Ni, 0.003% Ti, 0.006% O, 0.064% N, balance Fe) [5], respectively. The fusion zone geometry was simulated in each case using a well-tested, three-dimensional, numerical heat transfer and fluid flow code. Data used for the calculations are presented in Table 3. Figure 2a–c compare experimental and calculated spot weld geometry for arc welding of aluminum alloy 5182 [2], ($NaNO_3$) [3] and arc spot welding of steel [5], respectively. In each case the energy density of the heat source was such that no vapor-filled "keyhole" formed. Good agreement between the experimental and numerical predictions may be observed in the three cases. For the aluminum alloy 5182, although the thermal diffusivity is relatively high, convective heat transfer is still the main mechanism of heat transfer within the weld pool. Flow of liquid metal from the middle of the weld pool to its periphery on the top surface of the weld pool is driven by Marangoni convection. The flow forms one circulation loop of the weld metal and the resulting weld pool shape is hemispherical as shown in Figure 2a. For $NaNO_3$, the thermal diffusivity is low and the Prandtl number is high (8.1) [4]. Here, heat transfer and pool geometry is primarily controlled by strong convection currents. The fluid rushes to the edge and a strong return flow from the edge makes the periphery deeper than the center as can be observed from Figure 2b. Only one circulation loop forms in the weld pool. For the spot welding of steel, the Prandtl number is low (0.014) and the Marangoni number is very high (305,000). Here, the material has low thermal conductivity and convective heat transfer determines the shape of the weld pool. A wavy fusion boundary forms because of the two recirculation loops of the weld metal. The upper loop is shallow because of very large velocities driven by the strong Marangoni flow. This loop causes the liquid in the lower part along the weld centerline to recirculate in the opposite direction as shown in Figure 2c. The formation of two loops gives way to the formation of the unusual wavy fusion boundary with multiple inflections. The

Table 2. Dimensionless numbers obtained from the principal variables

$\pi_1 = (R)^{a_1} \cdot (\rho)^{b_1} \cdot (T_m)^{c_1} \cdot (\mu)^{d_1} \cdot C_P$	$a_1 = 2,\ b_1 = 2,\ c_1 = 1,\ d_1 = -2$	$\pi_1 = \frac{R^2\rho^2 T_m C_P}{\mu^2}$
$\pi_2 = (R)^{a_2} \cdot (\rho)^{b_2} \cdot (T_m)^{c_2} \cdot (\mu)^{d_2} \cdot k$	$a_2 = 2,\ b_2 = 2,\ c_2 = 1,\ d_2 = -3$	$\pi_2 = \frac{R^2\rho^2 T_m k}{\mu^3}$
$\pi_3 = (R)^{a_3} \cdot (\rho)^{b_3} \cdot (T_m)^{c_3} \cdot (\mu)^{d_3} \cdot \frac{d\gamma}{dT}$	$a_3 = 1,\ b_3 = 1,\ c_3 = 1,\ d_3 = -2$	$\pi_3 = \frac{R\rho T_m \frac{d\gamma}{dT}}{\mu^2}$
$\pi_4 = (R)^{a_4} \cdot (\rho)^{b_4} \cdot (T_m)^{c_4} \cdot (\mu)^{d_4} \cdot Q$	$a_4 = 1,\ b_4 = 2,\ c_4 = 0,\ d_4 = -3$	$\pi_4 = \frac{R\rho^2 Q}{\mu^3}$

Table 3. Welding parameters and material properties for arc spot welding of Al alloy 5182 [2], and for laser spot welding of $NaNO_3$ [3,4] and steel [5]

	Al 5182	$NaNO_3$	Steel
Power (W)	2500	12.4	1900
Beam radius (mm)	0.42	0. 75	1.2
Power distribution factor	2.0	2.0	1.5
Specific heat of solid (J kg^{-1} K^{-1})	898.7	1095.2	334.7
Viscosity (kg m^{-1} s^{-1})	1.1×10^{-3}	3.02×10^{-3}	1×10^{-3}
Thermal conductivity of solid (J m^{-1} s^{-1} K^{-1})	167.6	0.564	27.2
Density (kg m^{-3})	2300	1900	7800
Melting point (K)	850	580	1785
Enthalpy of melting (J kg^{-1})	3.95×10^5	1.8×10^5	2.67×10^5
Specific heat of liquid (J kg^{-1} K^{-1})	1199.7	1709.6	418.4
$d\gamma/dT$ (N m^{-1} K^{-1})	-3.5×10^{-4}	-5.9×10^{-5}	-5×10^{-4}
Thermal conductivity of liquid (J m^{-1} s^{-1} K^{-1})	107.8	0.564	29.3

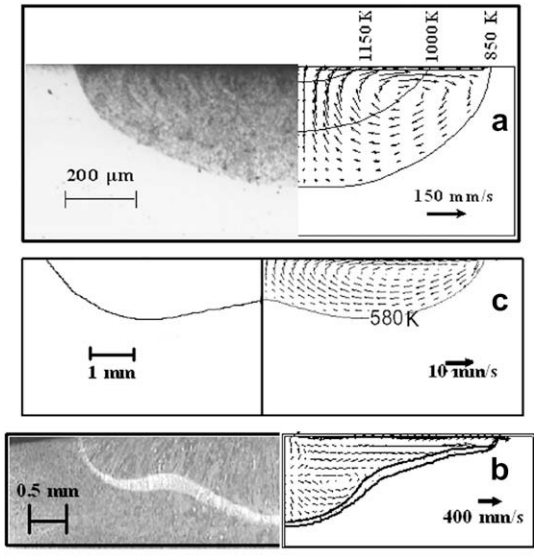

Figure 2. Comparison of experimental and calculated weld pool geometry for (a) arc welding of Al alloy 5182 [2], (b) laser melting of $NaNO_3$ [3,4] and (c) arc spot welding of steel [5]. The computed Prandtl numbers for the Al 5182 alloy, $NaNO_3$ and steel were 0.012, 8.21 and 0.014, respectively. The corresponding Marangoni numbers for the Al 5182 alloy, $NaNO_3$ and steel were 15400, 77,600 and 298,000, respectively, and the dimensionless heat inputs were 6.5, 45.4 and 30.3, respectively.

good agreements between the computed and the experimental weld fusion boundaries in all three cases indicate that the heat transfer and fluid flow model can correctly predict the fusion boundaries including the unusual wavy shape of the fusion boundaries.

In order to understand the welding variable and material property combinations that can result in wavy fusion boundary, several numerical runs were made using the heat transfer and fluid flow model, and the computed fusion boundaries were examined. Welding parameters and material properties were varied and dimensionless numbers were calculated in each case. The specific combinations of welding variables and material properties studied were selected on the basis of Taguchi's L64 orthogonal array. [19] The L64 array in its original form can have 21 columns (number of variables) for four different levels in every column. Here, the orthogonal array was used with nine variables with four levels for each variable. These nine variables, namely density (ρ), specific heat of liquid (C_P), thermal conductivity of liquid (k), viscosity of liquid (μ), melting temperature (T_m), temperature coefficient of surface tension ($d\gamma/dT$), beam radius (R), power distribution factor (d) and the absorbed power (Q), were found to significantly affect the appearance of wavy weld pool fusion boundary during preliminary studies using the heat and fluid flow model. The four different levels of the nine variables used are shown in Table 4.

The three meaningful dimensionless numbers, Pr, Ma, Q^*, derived with the help of the Buckingham π-theorem, are studied with respect to the geometry of weld pool and the appearance of inflections in the fusion boundary. In each case, the numerical heat transfer and fluid flow model was used to study the effect of thermophysical properties and welding parameters on the shape of the fusion boundary.

For high Prandtl number systems such as $NaNO_3$, the fluid flow pattern shows only one circulation loop. These materials are typically characterized by very low thermal conductivity and relatively low values of the temperature coefficient of surface tension, $d\gamma/dT$. As indicated above, the depth of the molten pool is wider near the periphery than in the middle. However, the inflection in the fusion zone boundary is perhaps most important for metallic systems with low Prandtl numbers.

In low Prandtl number systems, the dimensionless heat input was above 20 to ensure that a clearly defined

Table 4. Nine variables used for Taguchi's L64 array [19] with four levels of the values

Variable	Level 1	Level 2	Level 3	Level 4
Laser power (watt)	4500	5500	6500	7500
Beam radius (mm)	1.2	1.4	1.6	1.8
Power distribution factor	1.4	1.8	2.2	2.6
Viscosity (kg m^{-1} s^{-1})	5×10^{-4}	1×10^{-3}	1.5×10^{-3}	2×10^{-3}
Melting temperature (K)	1600	1700	1800	1900
Density (kg m^{-3})	7000	8000	9000	10,000
Specific heat of liquid (J kg^{-1} K^{-1})	837.3	1130.4	1423.5	1716.5
Thermal conductivity of liquid (J m^{-1} s^{-1} K^{-1})	41.8	83.7	125.6	167.4
Temperature coefficient of surface tension (N m^{-1} K^{-1})	1×10^{-4}	2.5×10^{-4}	4×10^{-4}	5.5×10^{-4}

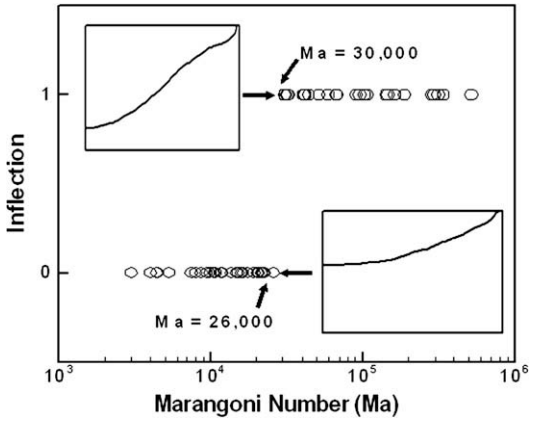

Figure 3. Influence of Marangoni number (Ma) on the appearance of wavy fusion zone boundary. On the *y*-axis, "1" indicates wavy nature and "0" represents no inflection in the fusion boundary. The insets show schematically the difference between the fusion boundary with and without the inflection.

fusion zone forms so that the shape of the fusion boundary can be well characterized. The Marangoni number was varied considerably. Figure 3 shows the appearance of inflection as a function of Marangoni number. The Marangoni numbers are indicated on the *x*-axis, whereas the *y*-axis represents the index for inflection: 1 = inflection in the fusion boundary; 0 = no inflection in the fusion boundary. The plot shows a clear distinction between the values of Ma for the appearance of wavy weld pool fusion boundary. It is observed that wavy weld pool fusion boundary appears only when Ma is higher than 26,000. In these cases with low *Pr*, the fusion zone is characterized by two recirculating loops of liquid metal that lead to the formation of the wavy boundary shown in Figure 1c.

The welding parameters and material properties responsible for the formation of an unusual, wavy fusion boundary with multiple inflections of its slope can be identified from heat and fluid flow calculations. Calculation of appropriate dimensionless numbers identified using the Buckingham π-theorem indicate that in metallic systems the wavy fusion zone boundary forms at a Marangoni number greater than 26,000 and a Prandtl number less than 0.06 for dimensionless heat input greater than 20. The wavy boundary originates from the interaction of counter-rotating liquid metal loops at high Marangoni numbers. High Prandtl numbers lead to inflections in the boundary with only one circulation loop.

[1] T. DebRoy, S.A. David, Reviews of Modern Physics 67 (1) (1995) 85–112.
[2] H. Zhao, T. DebRoy, Metallurgical and Materials Transactions B 32B (2001) 163–172.
[3] C. Limmaneevichitr, S. Kou, Welding Journal 79 (8) (2000) 231–237.
[4] A. Robert, T. DebRoy, Metallurgical and Materials Transactions B 32B (2001) 941–947.
[5] J.W. Elmer, T.A. Palmer, W. Zhang, T. DebRoy, Science and Technology of Welding and Joining 13 (3) (2008) 265–277.
[6] W. Liu, J. DuPont, Acta Materialia 52 (16) (2004) 4833–4847.
[7] M. Wolf, H. Schobbert, Th. Böllinghaus, in: Th. Böllinghaus, H. Herold (Eds.), Hot Cracking Phenomena in Welds, Springer Verlag, Berlin Heidelberg, New York, 2005, pp. 245–268.
[8] P.F. Mendez, T.W. Eager, in: J.M. Vitek, S.A. David, J.A. Johnson, H.B. Smartt, T. DebRoy (Eds.), Trends in Welding Research, ASM International, Materials Park, OH, 1998, pp. 13–18.
[9] P.W. Fuerschbach, Welding Journal 75 (1) (1996) 24s–34s.
[10] J.M. Drezet, S. Mokadem, Materials Science Forum 508 (2006) 257–262.
[11] J.M. Drezet, S. Pellerin, C. Bezençon, S. Mokadem, J. Phys. IV France 120 (2004) 299–306.
[12] W. Zhang, G.G. Roy, J.W. Elmer, T. DebRoy, Journal of Applied Physics 93 (5) (2003) 3022–3033.
[13] K. Mundra, T. DebRoy, K. Kelkar, Numerical Heat Transfer, Part A: Applications 29 (2) (1996) 115–129.
[14] X. He, P. Fuerschbach, T. DebRoy, Journal of Applied Physics 94 (10) (2003) 6949–6958.
[15] A. De, T. DebRoy, Journal of Applied Physics 95 (9) (2004) 5230–5239.
[16] A. De, T. DebRoy, Journal of Physics D: Applied Physics 37 (2004) 140–150.
[17] A. Kumar, T. DebRoy, Journal of Applied Physics 94 (2) (2003) 1267–1277.
[18] V. Streeter, E. Wylie, Fluid Mechanics, eigth ed., McGraw-Hill, New York, 1985.
[19] G. Taguchi, System of Experimental Design, Kraus,White Plains, NY, 1987.